Available online at www.sciencedirect.com
SCIENCE DIRECT®
PERGAMON
Applied Radiation and Isotopes 58 (2003) 501–508
Applied Radiation and Isotopes
www.elsevier.com/locate/apradiso

A 3D high-resolution gamma camera for radiopharmaceutical studies with small animals

G.K. Loudos[a,*], K.S. Nikita[a], N.D. Giokaris[b,c], E. Styliaris[b], S.C. Archimandritis[d], A.D. Varvarigou[d], C.N. Papanicolas[b,c], S. Majewski[e], D. Weisenberger[e], R. Pani[f], F. Scopinaro[f], N.K. Uzunoglu[a], D. Maintas[g], K. Stefanis[h]

[a] *Department of Electrical and Computer Engineering, Institute of Communication and Computer Systems, National Technical University of Athens, Iroon Polytexneiou 9, Str. Zografos, Attiki, 15773 Athens, Greece*
[b] *Institute of Accelerating Systems and Applications, P.O. Box 17214, 10024 Athens, Greece*
[c] *National Capodistrian University of Athens, Panepistimiou 30, 10679 Athens, Greece*
[d] *National Center for Scientific Research "Demokritos", Aghia Paraskevi, 15310 Athens, Greece*
[e] *Jefferson Lab, 12000 Jefferson Ave., Newport News, Virginia, USA*
[f] *University "La Sapienza", Rome, Italy*
[g] *Institute of Isotopic Studies, Distomou 5-7, Marousi, 15125 Athens, Greece*
[h] *University Mental Health Research Institute, Dimitressa 10, 11521, Athens, Greece*

Received 2 May 2002; received in revised form 11 November 2002; accepted 11 December 2002

Abstract

The results of studies conducted with a small field of view tomographic gamma camera based on a Position Sensitive Photomultiplier Tube are reported. The system has been used for the evaluation of radiopharmaceuticals in small animals. Phantom studies have shown a spatial resolution of 2 mm in planar and 2–3 mm in tomographic imaging. Imaging studies in mice have been carried out both in 2D and 3D. Conventional radiopharmaceuticals have been used and the results have been compared with images from a clinically used system.

Keywords: Small animal imaging; PSPMT; SPECT; High resolution; Radiopharmaceutical studies

1. Introduction

Over the past 30 years in vivo imaging with radiopharmaceuticals has proven to be an important diagnostic tool in nuclear medicine. Small animal imaging has been widely used for the evaluation of new radiopharmaceuticals. However, small animals are several times smaller than human subjects. In addition organs in small animals are 10 times (or more) smaller than those of a "standard" man.

Areas of extended research such as drug discovery and development use small animals for developing models of human diseases and in characterizing gene expression and phenotype changes that arise from genetic manipulations (Green et al., 2001). Over the years it has been realized that conventional systems do not meet the requirements in spatial resolution and sensitivity for this type of imaging. Dedicated systems based on Position Sensitive Photomultiplier Tubes (PSPMTs) or solid-state detectors have been developed during the past decade providing remarkable results in planar and tomographic mode (Kastis et al., 2001; Pani et al., 1997; Weisenberger et al., 1997).

Positron Emission Tomography (PET) systems (Watanabe et al., 1992) and Single Photon Emission

*Corresponding author. Tel.: +30-10-772-2285; fax: +30-10-772-3557.
E-mail address: gloudos@central.ntua.gr (G.K. Loudos).

0969-8043/03/$ - see front matter
doi:10.1016/S0969-8043(03)00025-3

Computed Tomography (SPECT) systems based on CdZnTe detectors (Kastis et al., 2001) have shown resolution of the order of 1–2 mm. Two-dimensional (2D) studies with PSPMTs have shown that a spatial resolution as high as 2 mm can be achieved (Pani et al., 1996). Few studies in SPECT imaging of phantoms or small animals using PSPMT's have also been reported (Matthews et al., 1995; Yasillo et al., 1994), showing their capability for successful small animal imaging.

The aim of the present work was to assess the performance of a small field of view (FOV) high-resolution PSPMT, suitable for small animal imaging, in both planar and tomographic mode. To this end phantom tests as well as experiments in normal mice, using conventional radiopharmaceuticals, have been carried out and compared with the images of a clinically used gamma camera in order to evaluate the system. A kinetic study in a tumor-bearing nude mouse using ^{99m}Tc-Bombesin is reported and SPECT images of the mouse kidneys are presented. Slices have been obtained by using Maximum Likelihood Expectation Maximization (ML-EM) algorithm, which is more robust to low number of counts and background noise (Loudos et al., 2001). Further acceleration in reconstruction process has been achieved by using an Ordered Subsets Expectation Maximization (OSEM) technique. Three-dimensional reconstruction from slices was carried out in real time using a Modified Marching Cubes (MMC) algorithm (Delibasis et al., 2001).

2. Methods

2.1. Equipment

The gamma camera consists of an R2486 Hamamatsu PSPMT equipped with two resistive chains connecting 8×8 crossed-wire anode wires. A 4.6 cm in diameter, 4 mm thick CsI(Tl) crystal, pixelized in 1.13 mm^2 squares and a 2.7 cm thick collimator with 1.22 mm diameter hexagonal parallel holes cells are used for photon detection.

The signals of the anodes are preamplified through 16 preamplifiers (LeCroy TRA1000) and then transferred to a CAMAC system, which hosts an Analogue to Digital Converter (ADC—LeCroy FERA 4300B), a memory (LeCroy FERA 4302), a driver (LeCroy FERA 4301) and a controller (Jorway 73A). The digital signals are transported to a G3 Power Mac via SCSI bus. The signal from the last dynode is inverted, amplified, passed through a discriminator (LeCroy 821) and used for ADC gating. Specific software (Kmax 6.4.5—Sparrow Corporation) allows CAMAC programming, system calibration, data acquisition and signal processing.

A computer-controlled step motor (MD-2 ARRICK Robotics) allows object rotation around the camera axis. Thus, projection data from several angles can be acquired. Fig. 1 shows the experimental configuration in tomographic mode.

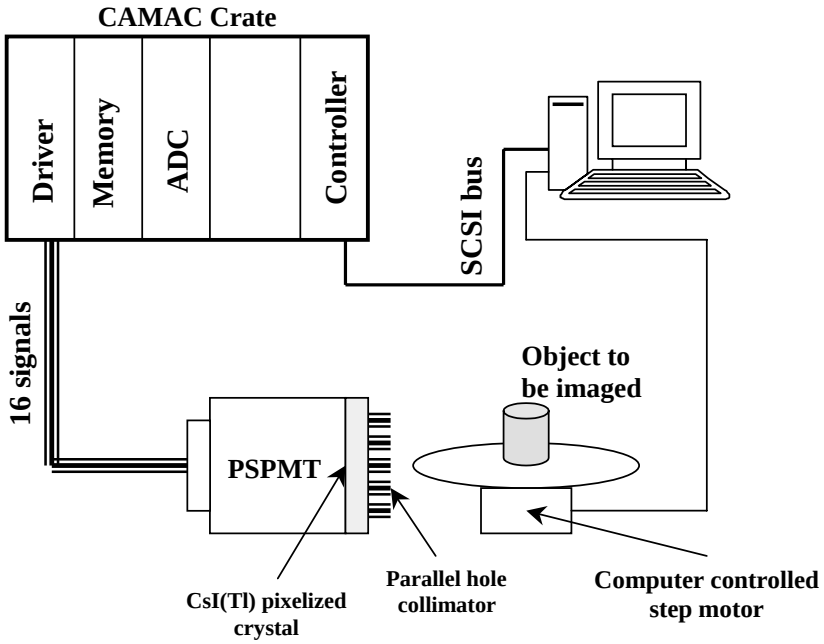

Fig. 1. Schematic diagram of the experimental setup.

2.2. Signal processing

The readout of the signals from a PSPMT has been extensively presented elsewhere (Weisenberger, 1998). An incident photon interacts with the CsI crystal and produces scintillation light. The pixelized crystal provides the advantage that scintillation does not spread laterally so much. The scintillation strikes the photocathode and liberates photoelectrons, which are multiplied at a 12-dynode system by an electric potential of typically 950 V, for ^{99m}Tc. Thus, an electron cloud reaches the crossed-wire anode stage. Readout of the 16 anode signals allows calculation of the Centre of Gravity (COG) of the electron cloud and consequently determination of the exact position of the incident photon in the XY plane. To avoid edge effects (Weisenberger, 1998), anode wires that carry small signals (less than 5% of the total anode signal) are disregarded in the COG calculation.

Calibration of the system is carried out using a flood source in order to correct non-uniformity in spatial efficiency of the crystal and the collimator. Pedestals subtraction of the ADC noise is also performed.

2.3. Slices reconstruction and 3D imaging

The projection data at each angle are a 41×41 matrix, determined by the number of the crystal's pixels in the main diameter. Each pixel corresponds to $1.13 \times 1.13\,\text{mm}^2$ in space. Since the crystal is circular, values of the data matrix near the corners are zero. Each line of the matrix represents projection data from one horizontal line and thus 41 slices can be reconstructed. However, due to insufficient number of crystal's pixels at the top and the bottom, the first and last three slices suffer from poor resolution and they are usually excluded from 3D reconstruction.

The object is rotated from 0° to 350° with a 10° step. In all tomographic acquisitions data are acquired for 5 min in each projection and corrections for ^{99m}Tc decay are performed. The slices of the object are reconstructed with ML-EM and OSEM acceleration technique is used. Details about these algorithms can be found in many references (Hudson and Larkin, 1994; Lange et al., 1987; Shepp and Vardi, 1982; Zeng, 2001) and they will not be described here. The reconstruction is performed on a standard Pentium III (800 MHz, 128MB) and the algorithms are implemented in MATLAB 5.3 environment. The MMC (Delibasis et al., 1999) algorithm allows efficient 3D reconstruction of the object from slices. As a result, the 3D reconstruction of the object can be viewed on a computer screen for further processing.

3. Results

3.1. Phantom imaging

In order to estimate the system spatial resolution in planar imaging, capillaries with inner diameter of 1.1 mm filled with ^{99m}Tc solution and placed at 2 mm distances from each other have been used. Planar images (Fig. 2a) obtained by positioning the camera close to the capillary phantoms and the corresponding line profiles have shown that a linear response and a 2 mm resolution is obtained in 2D, as expected. For the evaluation of system sensitivity to activity variations, a phantom consisting of eight holes (2 mm in diameter, 2 mm in depth) at 3 mm distances has been used. The holes have been filled with ^{99m}Tc solutions of relative activity ratios 1:1/2:1/3:1/4:1/5:1/6:1/7:1/8. The planar image and the line profile in the middle (Fig. 2b) have shown good agreement between the actual and the experimentally measured activity. In both cases acquisition time was 5 min and approximately 100,000 counts were collected.

The system spatial resolution has been estimated in tomographic mode as well. Experiments have been performed using capillaries (1.1 mm i.d.) placed at intercapillary distances of 5, 3.5 and 2 mm. Slices reconstruction has been carried out using an ML-EM algorithm. A total of 50 iterations and about 50 s was sufficient. By using OSEM with nine subsets and two iterations, the same image quality was obtained in 12 s.

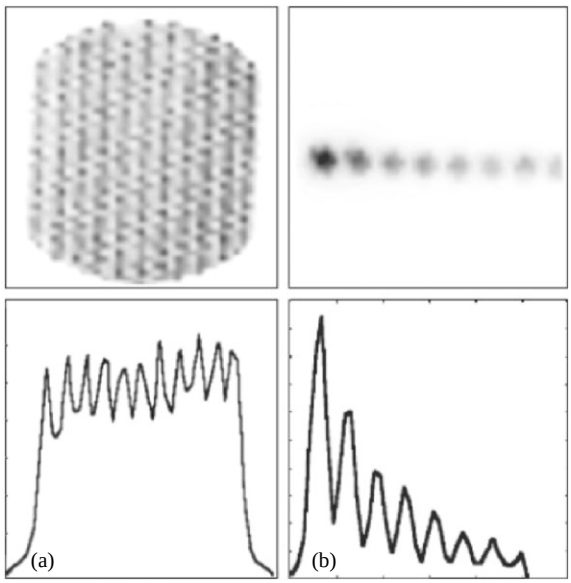

Fig. 2. (a) Eleven capillaries (1.1 mm inner diameter—i.d.) filled with the same ^{99m}Tc solution and their typical line profiles. (b) A phantom consisting of eight holes (2 mm in diameter, 2 mm in depth) at 3 mm distances filled with ^{99m}Tc solutions of relative activity ratios 1:1/2:1/3:1/4:1/5:1/6:1/7:1/8.

In Fig. 3, a typical slice and its corresponding line profile is shown. As it can be seen the first three capillaries can be clearly distinguished while the fourth capillary is also visible.

3.2. Small animal imaging

Extensive comparative mice studies with a hospital gamma camera equipped with a pinhole collimator (single head, ZLC Orbiter, SIEMENS) have been performed using ^{99m}Tc-labeled conventional radiopharmaceuticals. In Fig. 4a, a detailed picture of a mouse skeleton after the injection of 0.25 mCi of ^{99m}Tc-MDP has been obtained with the developed system. The same mouse has been imaged with the clinically used system (Fig. 4b). In Fig. 4c, mouse kidneys are imaged after the injection of 0.25 mCi of ^{99m}Tc-DMSA. Kidneys are well separated and the pelvis is visible at the bottom of the image. On the other hand, in the conventional scintigram (Fig. 4d) most of the details are lost. Acquisition time was 10 min for both systems; 50,000 counts were collected with the PSPMT detector and 400,000 with the clinical system, respectively.

The system has proven to be suitable for imaging other isotopes with similar energies. In Fig. 5a a small tumor, which lies below the kidneys and over the bladder, is imaged with ^{153}Sm–DTPA–anti-CEA, which had been developed for therapeutic purposes. The injected dose was 0.5 mCi. In Fig. 5b, a tumor below the kidneys is imaged using 0.5 mCi of ^{188m}Re-Lanreotide. In both cases the developed system has been used in order to test the tumor uptake of the derivatives. Acquisition time was 10 min and 50,000 counts were collected.

The system has been successfully used for dynamic studies. In order to evaluate a ^{99m}Tc-Bombesin analogue (Varvarigou et al., 2003) a tumor-bearing nude mouse has been imaged. The injected dose was 0.5 mCi. The in vivo studies were performed in compliance with the European legislation. Animal protocols have been approved by the Hellenic authorities. Nine consecutive images are shown in Fig. 6. First and last images were taken 30 and 180 min post-injection (p.i.), respectively.

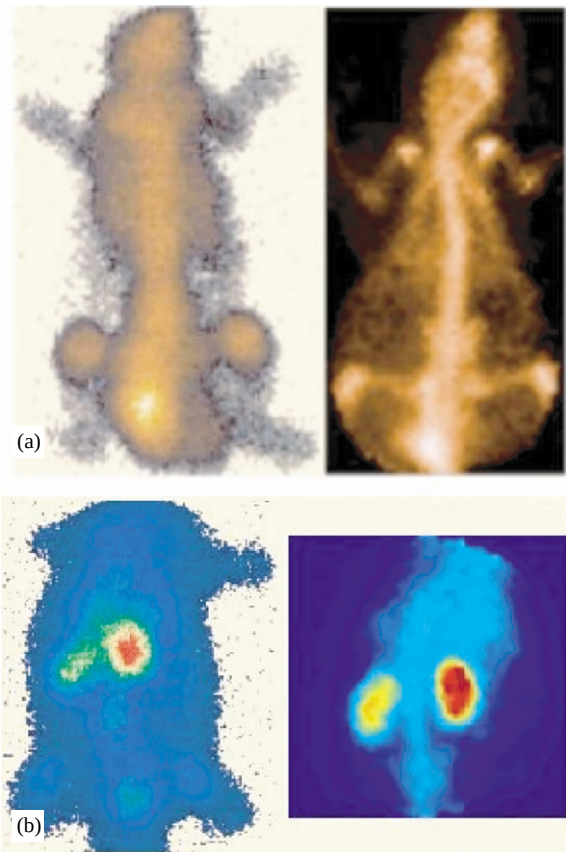

Fig. 4. (Top) A mouse injected with 0.25 mCi of ^{99m}Tc-MDP and imaged with (a) the PSPMT system and (b) a clinically used gamma camera equipped with a pinhole collimator. (Bottom) A mouse injected with 0.25 mCi of ^{99m}Tc-DMSA. Comparative images of (c) the PSPMT system and (d) the hospital pinhole collimator (right).

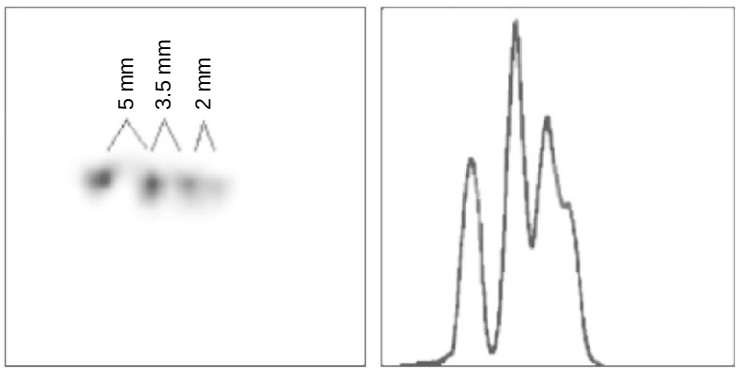

Fig. 3. A slice and a line profile of four capillaries placed at intercapillary distances of 2, 3.5 and 5 mm. The slices are reconstructed using OSEM.

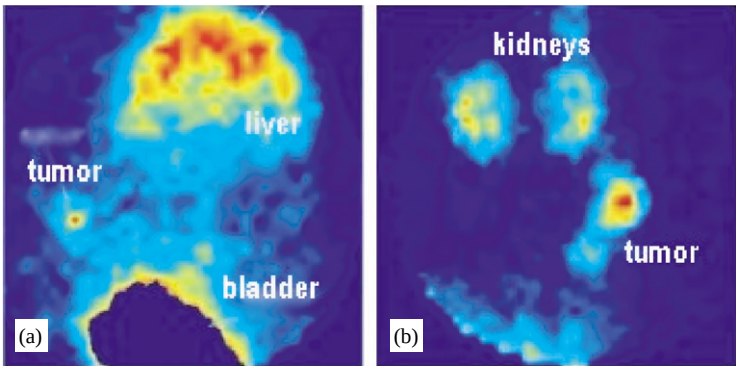

Fig. 5. (a) Mouse injected with 0.5 mCi of ^{153}Sm–DTPA–anti-CEA and (b) with 0.5 mCi of ^{188m}Re-Lanreotide.

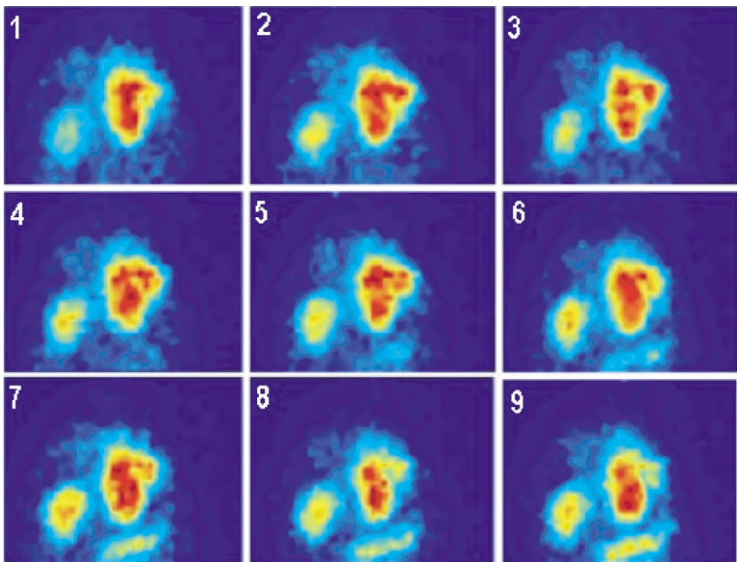

Fig. 6. Dynamic evaluation of a ^{99m}Tc-Bombesin analogue. The injected dose was 0.5 mCi. Nine consecutive images from 30 to 180 min p.i. are shown. Five minutes acquisition is carried out for each image with 10 min intervals between images. The tumor is seated below kidneys and the bladder is masked.

Data have been acquired for 5 with 10 min intervals and approximately 30,000 counts were collected. The experimentally induced tumor is seated below the kidneys and it starts being visible in the fifth image—105 min p.i.—with maximum uptake at 165 min p.i. No remarkable change is observed in the last image.

Next, the ability of the system for 3D imaging of small animal organs has been assessed. In Fig. 7a, a planar image of a normal mouse injected with 0.5 mCi of a ^{99m}Tc-Bombesin analogue is shown. The mouse is placed under the camera in a typical position for 2D imaging. No organs can be distinguished, because ^{99m}Tc-Bombesin is concentrated both in kidneys and bowels that are located in different depths. Then the animal was placed in position for tomographic acquisition. Data were collected for 5 min, as described in section IIC and approximately 30,000 were collected per projection. Thirty-five slices have been obtained using OSEM and 3D reconstruction has been carried out using MMC. The 3D views of Fig. 7b indicate concentration of the labeled derivative in the kidneys and the bowels, which are clearly separated.

Moreover kidney imaging of a mouse injected with 0.25 mCi of ^{99m}Tc-DMSA has been carried out and the obtained 3D reconstruction is shown in Fig. 8. Again 30,000 counts were acquired in 5 min per projection. A good depiction of both kidneys and part of the spine can be easily observed.

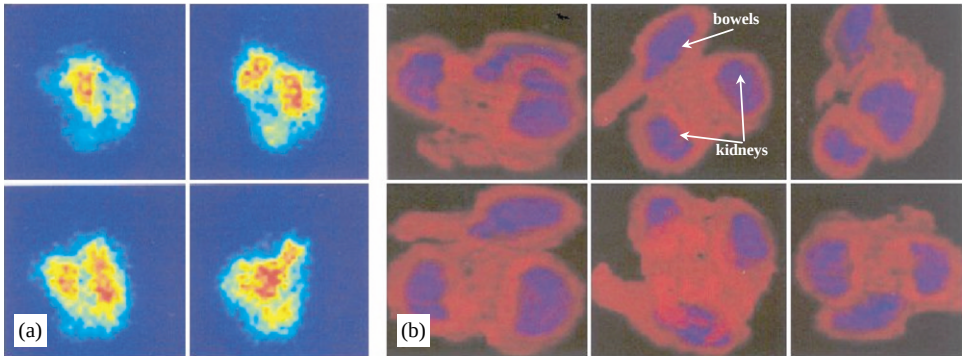

Fig. 7. Comparative (a) 2D and (b) 3D images of a normal mouse injected with 0.5 mCi of ^{99m}Tc-Bombesin. In the planar images no organs can be separated since ^{99m}Tc-Bombesin is concentrated both in kidneys and bowels that are located in different depths. In the 3D images both kidneys and part of the bowels can be clearly distinguished.

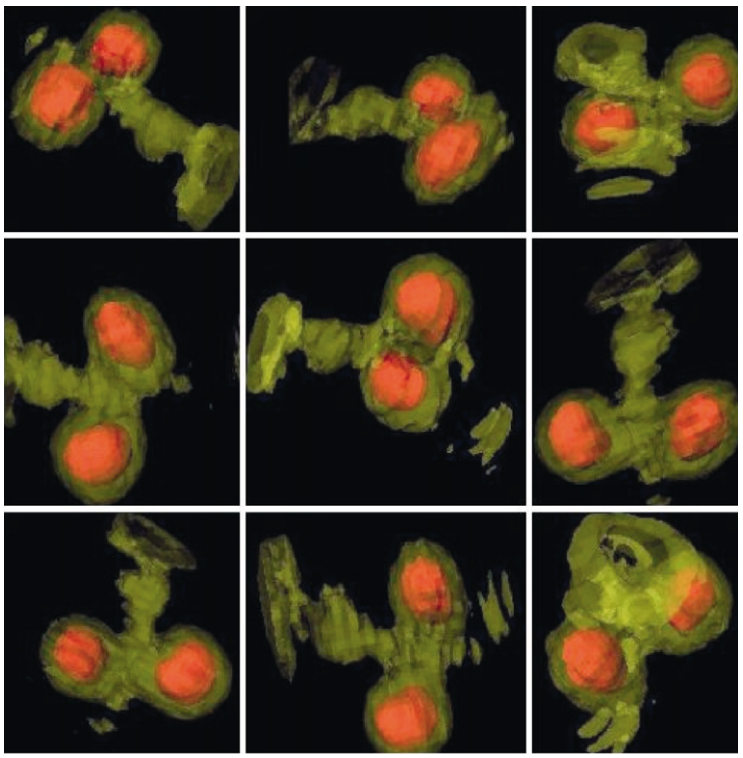

Fig. 8. SPECT kidneys imaging of a normal mouse injected with 0.25 mCi of ^{99m}Tc-DMSA.

4. Discussion

Planar imaging is widely used in radiopharmaceuticals' evaluation. However, projection data take into account the contribution of all the sources that are seated at different depths. Subsequently, in case that a radiopharmaceutical concentrates to more than one organs (e.g. kidneys–liver) or structures (e.g. kidneys–tumor), 2D imaging fails to provide adequate information. On the contrary, 3D imaging permits exact localization of the independent sources that can be found in an object from a sufficient number of planar images.

The use of a single camera has the disadvantage of high acquisition time; we have shown in a phantom study (Varvarigou et al., 2003) that 2 h of acquisition are usually necessary in order to obtain 36 projections with a satisfactory number of counts (which is about 100

counts/mm^2 of the detector area) are necessary. In case of ^{99m}Tc, decay correction has to be carried out, depending on acquisition time and isotope activity. A second camera can reduce the acquisition time by a factor of two and a system based on more cameras can be used in order to perform short time examinations. Thus, kinetic studies in 3D can be performed and radiopharmaceuticals evaluation can be carried out in a more precise way.

Clinical SPECT systems use Filtered Backprojection (Kak and Slaney, 1987) (FBP) algorithm for slices reconstruction. However, FBP is sensitive to noise, low number of counts and low number of projections and produces image artifacts, which reduce resolution. On the other hand, statistical algorithms based on Maximum Likelihood Estimation and other iterative techniques seem to give superior results. Despite their computational cost, they provide the advantage that attenuation and scattering information can be included in the system matrix and thus more accurate images can be reconstructed. The continuous progress in computer technology has made possible the implementation and fast performance of these algorithms in commercially available PCs.

The small FOV gamma camera, which is determined by crystal size (4.5 cm in diameter), can only be used for small animal imaging, especially in SPECT, where the detector must view the whole object at every angle. PSPMTs with a larger FOV are already commercially available, offering a spatial resolution of about 2 mm in planar studies (Wojcik et al., 1998). A larger FOV system based on PC electronics is under development. In addition, we are in the process of optimising the iterative algorithms by including attenuation and scattering corrections in reconstruction process.

Since a 2–3 mm resolution can be achieved in 3D, it seems that a larger FOV detector can be used for small human organs imaging as well. Scintimammography is a clinical field where PSPMTs are being tested lately (Giokaris et al., 2003; Majewski et al., 1998). A SPECT camera based on PSPMTs will allow early detection and exact localization of possible small size tumors, providing useful information for diagnostic and therapeutic purposes.

5. Conclusion

PSPMTs can be used for the development of a low-cost small animal SPECT detector with a high resolution of the order of 2–3 mm. The promising results in these animal studies clearly indicate that this technique can play a significant role in radiopharmaceuticals evaluation with possible applications in Nuclear Medicine.

Acknowledgements

The authors would like to thank the National and Kapodistrian University of Athens Special Account for Research Grants.

References

Delibasis, K.K., Matsopoulos, G., Mouravliansky, K.N., Nikita, K.S., 1999. Efficient implementation of the marching cubes algorithm for rendering medical data. In: Sloot, P., Buldak, M., Hoekstra, A., Hertzeberger, B. (Eds.), Proceeding of the Seventh International Conference, Lecture Notes in Computer Science, High Performance Computing and Networking, HPNC. Springer, Amsterdam, The Netherlands, pp. 989–999.

Giokaris, N., Loudos, G., Maintas, D., Papapanagiotou,. D., Nikita, K., Uzunoglu, N., Karabarbounis, A., Papanicolas, C., Stiliaris, E., Archimandritis, S., Varvarigou, A., Stefanis, C., Majewski, S., Weisenberger, D., Pani, R., Scopinaro, F., 2003. 3D imaging of breast phantoms using a high resolution position sensitive photomultiplier tube. Nuclear Instruments and Methods in Physics Research Section A: Accelerators, Spectrometers Detectors and Associated Equipment, Volume 497, Issue 1, pp. 141–149.

Green, M.V., Seidel, J., Vaquero, J.J., Jagoda, E., Lee, I., Eckelman, W.C., 2001. High resolution PET, SPECT and projection imaging in small animals. Comput. Med. Imaging Graphics 25, 79–86.

Hudson, H.M., Larkin, R.S., 1994. Accelerated image reconstruction using ordered subsets of projection data. IEEE Trans. Med. Imaging 13 (4), 601–609.

Kak, C., Slaney, 1987. Principles of Computerized Tomographic Imaging. IEEE Press, New York.

Kastis, G.A., Wu, M.C., Balzer, S.J., Wilson, D.W., Furenlid, L.R., Stevenson, G., Barber, H.B., Barrett, H.H., Woolfenden, J.M., Kelly, P., Appleby, M., 2001. Tomographic small-animal imaging using a high resolution semiconductor camera. 2000 IEEE Conference Record. Nucl. Sci. Symp. Med. Imaging Conf. 3, 2629–2633.

Lange, K., Bahn, M., Little, R., 1987. A theoretical study of some maximum likelihood algorithms for emission and transmission Tomography. IEEE Trans. Med. Imaging 6, 106–114.

Loudos, G., Nikita, K., Uzunoglu, N., Mouravliansky, N., Matsopoulos, G., 2001. Performance of iterative reconstruction algorithms for small organs high resolution SPECT imaging using a PSPMT based detector. Book of Abstracts, European Association of Nuclear Medicine, Napoli, p. 970, 25–29 September 2001.

Majewski, S., Farzanpay, F., Goode, A., 1998. Development of an application specific scintimammography detector based on a crystal scintillator array and a PSPMT. Nucl. Instrum. Methods A 409, 520–523.

Matthews, K.L., Aarsvold, J.N., Heimsath, S.J., Yasillo, N.J., Chen, C.T., 1995. Tomographic imaging with a miniature gamma camera. 1994 IEEE Conference Record. Nucl. Sci. Symp. Med. Imaging Conf. 3, 1292–1296.

Pani, R., Pellegrini, R., Soluri, A., De Vincentis, G., et al., 1996. First results from YAP: Ce gamma camera for small animal studies. IEEE Trans. Nucl. Sci. 43 (6), 3264–3271.

Pani, R., Pellegrini, R., Scopinaro, F., et al., 1997. Scintillating array gamma camera for clinical use. Nucl. Instrum. Methods A 392, 295–298.

Shepp, L.A., Vardi, Y., 1982. Maximum likelihood reconstruction for emission Tomography. IEEE Trans. Med. Imaging 1 (2), 113–121.

Varvarigou, A.D., Scopinaro, F., Leondiadis, L., Corleto, V., Schillaci, O., De Vincentis, G., Sourlingas, T.G., Sekeri-Pataryas, K.E., Evangelatos, G.P., Leonti, A., Datseris, J., Xanthopoulos, S., Delle Fave, G., Archimandritis, S.C., 2002. Synthesis, chemical, radiochemical and radiobiological evaluation of a new ^{99m}Tc-labelled Bombesin-like Peptide. Cancer Biotherapy and Radiopharmaceuticals 17, 317–326.

Watanabe, M., Uchida, H., Okada, H., Shimizu, K., et al., 1992. A high resolution PET for small animal studies. IEEE Trans. Med. Imaging 11 (4), 577–580.

Weisenberger, A. 1998. Gamma ray imaging detector for small animal research. Ph.D. Dissertation, The College of William and Mary in Virginia.

Weisenberger, A., Majewski, S., Saha, M., Bradley, E., 1997. Coincident radiation imaging of iodine 125 for in vivo gene imaging in small animals. Nucl. Instrum. Methods A 392, 299–303.

Wojcik, R., Majewski, S., Kross, B., Steinbach, D., Weisenberger, A., 1998. High spatial resolution gamma imaging detector based on a 5″ diameter R3292 Hamamatsu PSPMT. IEEE Trans. Nucl. Sci. 45, 487–491.

Yasillo, N.J., Mintzer, R.A., Aarsvold, J.N., Beck, R.N., Block, T.A., Chen, C.-T., Cooper, M., Heimsath, S.J., Matthews, K.L., Ordonez, C.E., Pan Wu, C., 1994. A single-tube gamma camera for clinical imaging, 1993 IEEE conference record. Nucl. Sci. Symp. Med. Imaging Conf. 3, 1073–1076.

Zeng, G.L., 2001. Image reconstruction—a tutorial. Comput. Med. Imaging Graphics 25, 97–103.